Effects of Nanoparticle Shape on the Morphology and Properties of Porous CdSe Assemblies (Aerogels)

Hongtao Yu and Stephanie L. Brock*

Department of Chemistry, Wayne State University, Detroit, Michigan 48202

ARTICLE

ABSTRACT We demonstrate the effect of differently shaped CdSe nanoscale building blocks (dots, rods, branched nanoparticles, and hyperbranched nanoparticles) on the morphologies, surface characteristics, and optical properties of resultant porous CdSe nanostructured aerogels. Monolithic CdSe aerogels were produced by controlled oxidative removal of surface thiolate ligands from differently shaped CdSe nanoparticles to yield a wet gel, followed by CO_2 supercritical drying. The X-ray diffraction data show that the resultant CdSe aerogels maintain the crystalline phase of the building blocks without significant grain growth. However, the transmission electron microscopy images indicate that the morphology of CdSe aerogels changes from a colloid-type morphology to a polymer-type morphology when the building block changes from dot to rod or the branched nanoparticle. The morphology of the CdSe aerogel assembled from hyperbranched nanoparticles appears to be intermediate between the colloid-type and the polymer-type. Nitrogen physisorption measurements suggest that the surface areas and porosity are a direct function of the shape of the primary building blocks, with aerogels formed from rods or branched particles exhibiting the greatest surface areas (>200 m^2/g) and those prepared from hyperbranched nanoparticles exhibiting the least (<100 m^2/g). Band gap measurements and photoluminescence studies show that the as-prepared CdSe aerogels retain to a large extent the intrinsic quantum confinement of the differently shaped building blocks, despite being connected into a 3D network.

KEYWORDS: CdSe nanomaterials · colloidal aerogel · polymeric aerogel · porous structures · quantum confinement

Recent advances in the precise control of the size,[1] shape,[2] composition,[3] and surface chemistry[4] of inorganic nanoparticles have enabled a second stage of nanoparticle research, assembly of nanoparticles into functional architectures, to be more and more important. Nanoparticle assembly methods serve as a powerful tool to connect nanoscale building blocks into complex macroscopic architectures. A novel concept in which sphere-shaped inorganic nanoparticles are treated as artificial atoms has led to a successful self-assembly strategy to organize the inorganic nanoparticles into superlattices with similar bulk crystalline structures[5] to atomic solids, resulting in novel collective properties.[6,7] Further, varying the size ratio of two kinds of nanoparticles and tuning the charge state of the nanoparticles by exchanging the surface ligands results in structurally diverse binary nanoparticle superlattices.[8,9] However, from a device performance perspective, the interaction between the particles in such superlattices is necessarily mediated by surface ligands. These surface ligands may be detrimental to electrical transport properties and harmful to the thermal stability of the artificial solid.

Aerogels, with their low density, high surface areas, and large open pores, are a unique class of inorganic polymers.[10] However, traditional aerogel research has focused largely on metal oxides,[11–15] with the extension of sol−gel methods to the preparation of chalcogenide aerogels only recently realized.[16–24] We have adopted the aerogel as an architectural model for the creation of functional 3-D linked quantum dots. To realize this model, we have developed a general methodology to assemble metal chalcogenide nanoparticles into nanostructures by controlled oxidative removal of surface thiolate ligands, followed by supercritical drying to retain the structure of the wet gel.[16,17,19–23,25] This powerful assembly strategy not only adds new members to the traditional aerogel family but also represents a novel and effective way to organize the metal chalcogenide nanoparticles into 3D architectures without the presence of intervening ligands that can potentially limit the electron transport properties and thermal stability.

In this contribution, we employ a new strategy to systematically vary the morphology and properties of metal chalcogenide aerogels by altering the shape of the primary nanoparticle in the CdSe system. CdSe nanoparticles have gained extensive attention from material scientists due to the

*Address correspondence to sbrock@chem.wayne.edu.

Received for review April 18, 2008 and accepted June 27, 2008.

Published online July 15, 2008.
10.1021/nn8002295 CCC: $40.75

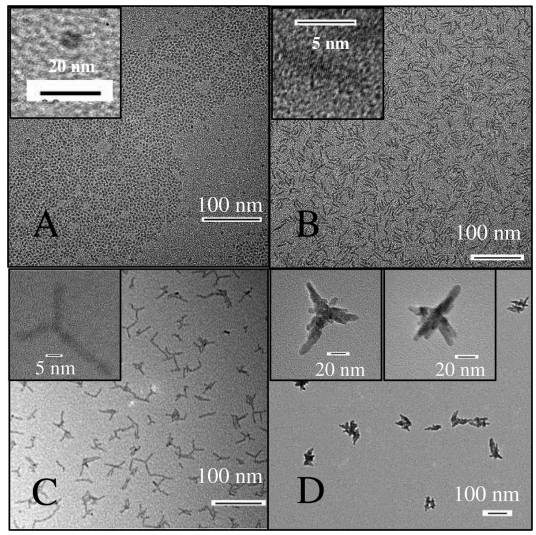

Figure 1. TEM images of the four kinds of nanoscale CdSe building blocks used in the present study: (A) dots (3.17 ± 0.31 nm), (B) rods (3.40 ± 0.33 × 22.7 ± 2.2 nm), (C) branched nanoparticles (body width = 4.6−5.0 nm; arm length = 18.8−28.8 nm), and (D) hyperbranched nanoparticles (body width = 6.5−6.9 nm; arm length = 23.3−36.7 nm). The insets are HRTEM images of single particles.

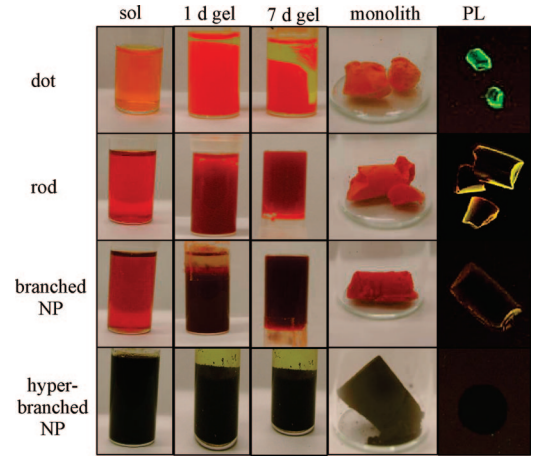

Figure 2. Images of CdSe nanoparticle sols, gels (1 and 7 day aging times), and monolithic aerogels as a function of the shape of the primary particle; corresponding photoluminescence (PL) images of monolithic aerogels acquired under UV stimulation in the dark are shown at far right. Seven day aged gels of rod and branched particles are shown inverted in their molds.

relative ease of synthesis, the ability to precisely control the size and shape, and the ensuing optical properties. Here, we take advantage of diverse synthetic techniques to achieve differently shaped CdSe nanoparticles and assemble them into porous 3D aerogel networks in order to study how the shape of the building block influences the morphology and properties of the resultant aerogels. A comparison of the properties of dot and rod aerogels has been previously published as a communication.[26]

RESULTS AND DISCUSSION

CdSe nanoparticles with different shapes (dot, rod, branched, and hyperbranched) were synthesized by employing variations of a typical high temperature arrested precipitation technique.[1] Coordinating solvents with high boiling points, such as trioctylphosphine oxide (TOPO) and trioctylphosphine (TOP), were used as the synthetic media for control of particle growth. A low precursor concentration and slow growth rate employing a small amount of tetradecylphosphonic acid (TDPA) to dissolve the Cd precursor (CdO) favor the thermodynamic growth of the nanoparticles, therefore leading to the formation of isotropic sphere-shaped CdSe nanoparticles, in which the surface energy is minimized relative to anisotropic shapes (Figure 1A).[27] Alternatively, a high precursor concentration and fast growth rate employing relatively large amounts of TDPA, which exhibits preferential binding to the (100) CdSe crystal facets,[27] result in a kinetic growth regime, therefore favoring the formation of anisotropic rod-shaped CdSe nanoparticles (Figure 1B). Branched CdSe nanoparticles were synthesized *via* first preparing CdSe tetrahedron-shaped nuclei of cubic crystalline phase at low temperature (160 °C), then facilitating fast growth of the hexagonal arms outward at a tetrahedral angle by gradually increasing the temperature to 230 °C (Figure 1C).[27] Hyperbranched CdSe nanoparticles were synthesized by adding a bifuntional ligand, 2-carboxyethylphosphonic acid (CEPA), which favors the formation of basic branching points on the existing nanoparticle surfaces (Figure 1D).[28]

CdSe aerogels assembled from differently shaped building blocks were prepared by first exchanging the as-prepared nanoparticles (presumably capped with TOP/TOPO and/or TDPA/CEPA) with thiolate ligands

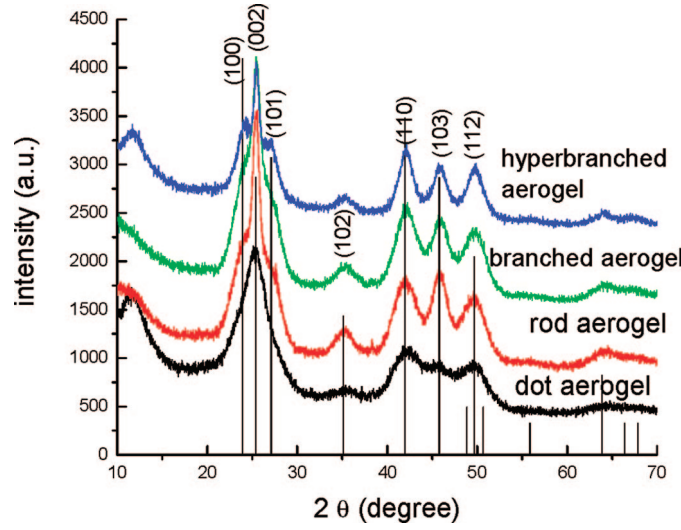

Figure 3. Powder X-ray diffraction patterns for the four kinds of CdSe aerogels investigated. The vertical lines are from PDF file # 08-0459 (hexagonal CdSe).

TABLE 1. BET Surface Areas, Silica Equivalent Surface Areas Based on Relative Density Calculations, BJH Adsorption Average Pore Diameters, and BJH Cumulative Pore Volumes of the Four Kinds of CdSe Aerogel (Data Averaged from Three Individual Samples), Along with Aerogel Composition (Atomic Ratio) from TEM-EDS and Band Gap Values of Building Blocks *versus* Resultant Aerogels

CdSe aerogel	BET surface area (m^2/g)	silica equivalence (m^2/g)	average pore diameter (nm)	cumulative pore volume (cm^3/g)	atomic ratio from TEM-EDS: Cd/Se/S/P	band gap values: building block/aerogel (eV)
dot aerogel	105 ± 10	251 ± 26	35.4 ± 2.4	0.63 ± 0.13	47.2/47.3/5.5/ND	2.15/2.12
rod aerogel	241 ± 6	576 ± 13	25.1 ± 1.5	1.64 ± 0.11	48.0/46.8/5.3/ND	2.06/2.01
branched aerogel	227 ± 12	543 ± 28	22.3 ± 1.9	1.39 ± 0.06	45.6/48.8/5.5/ND	2.03/1.99
hyperbranched aerogel	79 ± 2	189 ± 3	13.2 ± 0.7	0.26 ± 0.03	48.5/48.2/2.4/0.9	1.83/1.81

(11-mercaptoundecanoic acid in the presence of base). Controlled oxidative removal of the surface thiolate ligands by adding an oxidizing agent (3% tetranitromethane) yielded wet gels, followed by supercritical CO_2 drying to yield the aerogel. Like traditional silica aerogels, the CdSe aerogels can be prepared as monoliths (molded from gel form, Figure 2) with very low densities (0.1−0.2 g/cm^3, monolith mass over estimated volume); however, unlike traditional silica aerogels, the aerogels made from CdSe nanoparticles are crystalline due to the high crystallinity of the building blocks. All the powder X-ray diffraction patterns of CdSe aerogels prepared from differently shaped building blocks demonstrate the identical hexagonal (cadmoselite) crystalline phase, consistent with the crystal structure of their building blocks (Figure 3). The presence of much sharper peaks, and the resolution of the (100) and (101) peaks, upon progressing from the pattern for the CdSe dot aerogel to that of the hyperbranched aerogel are reflective of an increase in size of the building blocks. The sharpness of the (002) peaks in the patterns of the rod, branched, and hyperbranched nanoparticles and aerogels indicates that the principal direction of crystal growth is along the *c*-axis, as expected.[27] A small but sharp peak near 38° in 2θ is observed occasionally, which matches CdO (Monteponite, PDF: 05-0640), and may be attributed to incomplete dissolution/reaction of the CdO precursors. Energy dispersive spectroscopy measurements indicate an overall Cd:Se ratio of 1:1 with 2.4−5.5 atomic % sulfur and little or no phosphorus (Table 1). These data are consistent with the expected composition of CdSe, plus the presence of some residual thiolate surface functionalities.

Transmission electron microscopy was employed to image the morphology of the prepared aerogels from differently shaped building blocks (Figure 4). The resultant aerogels exhibit two major gel morphologies. CdSe aerogels assembled from dot-shaped nanoparticles display a colloidal morphology, similar to that of base-catalyzed silica aerogels. On the other hand, aerogels assembled from rod or branched nanoparticles exhibit a polymeric morphology, similar to acid-catalyzed silica aerogels. The morphology of the CdSe aerogel assembled from hyperbranched nanoparticles appears to be intermediate between the colloidal-type and the polymer-type. To achieve different morphologies in silica aerogels, the kinetics of hydrolysis and condensation must be varied.[29] In the present case, we show that varying the shape of the building block used in metal chalcogenide gel formation is an alterna-

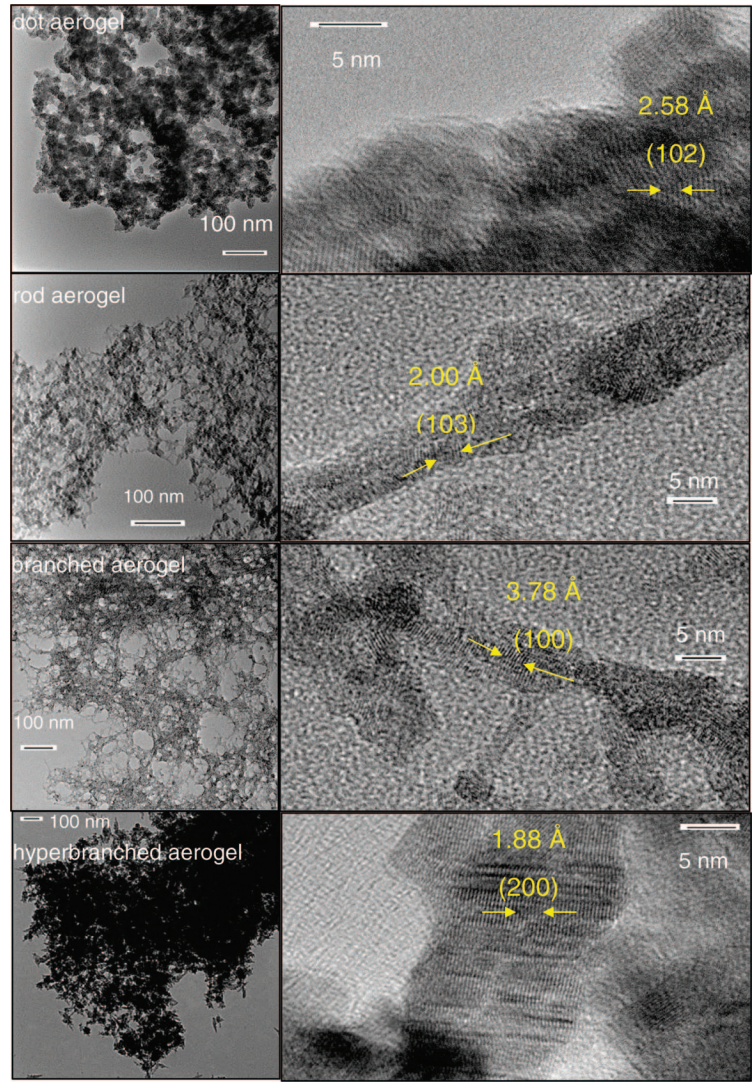

Figure 4. TEM images of the four kinds of CdSe aerogels investigated (left, low magnification; right, high resolution). Arrows indicate groups of lattice fringes; individual fringe spacing and corresponding indices to hexagonal CdSe are given.

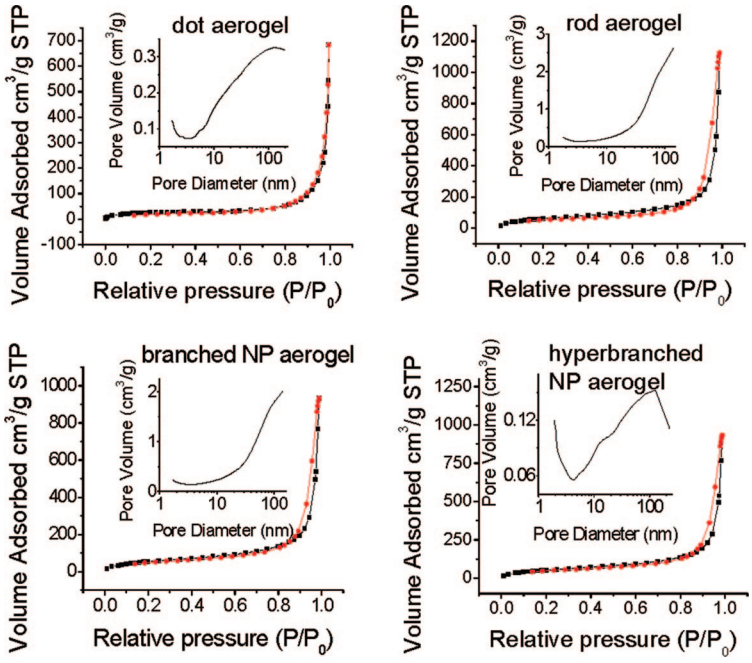

Figure 5. Nitrogen adsorption (black filled squares)/desorption (red filled circles) isotherms for the four kinds of CdSe aerogels investigated. The insets show pore size distributions based on BJH modeling of adsorption isotherms.

tive way to tune the morphology of the aerogel, thereby enabling more control over the resultant morphology. The origin of the polymeric morphology obtained from rod or branched nanoparticles may be directly related to the different surface free energies of crystal faces in these structures. Specifically, the end points of rod or branched nanoparticles are more chemically reactive than the faces of the arms due to the presence of more available dangling bonds on the end facet,[27] enabling dissimilar materials, such as gold or CdTe nanodots, to be preferentially deposited onto the end points.[30,31] We postulate that this difference of surface free energy as a function of the nanocrystal facet plays a significant role in the networks formed from CdSe rods or branched nanoparticles. End to end connections lead to a more penetrating network for CdSe rod or branched aerogels, relative to dot aerogels. The presence of end to end connected joints is visible in HRTEM images of rod and branched aerogels (Figure 4) in addition to some interweaving of the rod/branched arms to form reinforced struts. This leads to enhanced gel strength and minimal gel contraction, as previously noted.[12] Thus, gels prepared from rods or branched nanoparticles maintain the volume of the sol and can be inverted without fragmenting, in contrast to gels prepared from dots (Figure 2, 7 day gels). The morphology of the CdSe aerogel assembled from hyperbranched nanoparticles is similar to the colloidal aerogels in that large spheroid features are apparent, but these are connected together *via* the high-aspect ratio arms, and thus the hyperbranched aerogel has clear aspects of the polymeric aerogel morphology, as well. While the gel does not undergo the contraction (syneresis) noted for the dot gels, it is a considerably weaker gel than those obtained from rods and branched nanoparticles and must be handled very carefully to retain the monolith throughout the critical point drying. HRTEM images also testify to the crystallinity noted in the PXRD; lattice fringes are clearly evident and can be indexed to hexagonal CdSe in all cases.

The surface areas and pore size distributions of CdSe aerogels assembled from differently shaped building blocks were obtained by analysis of nitrogen adsorption/desorption isotherms (Figure 5). The data were fit to a Brunauer–Emmett–Teller (BET) model to determine the surface areas of the CdSe aerogels. The pore size distribution, average pore diameter, and cumulative pore volumes were calculated from the Barrett–Joyner–Halenda (BJH) model (based on cylindrical pores). The density functional theory module of the Micromeritics software was also applied to calculate the pore size distribution over the complete range of the isotherm (BJH is limited to pore diameters $\geq$2 nm). This method is based on calculating the equilibrium density profile of the gas molecule during each step of the adsorption process and assumes a slit-shaped pore geometry. These data are presented in Table 1. To compare the obtained surface areas directly to those of traditional silica aerogels, the silica equivalent surface areas based on the relative densities of wurzite CdSe and silica were also computed and are shown in Table 1.

The adsorption/desorption isotherms generated for CdSe aerogels are similar in shape, regardless of the differing shapes of the building block (Figure 5), and represent a type IV curve, characteristic of a mesoporous (2–50 nm pore diameter) material,[32,33] with a sharp upturn in the high relative pressure region, which indicates liquid condensation associated with the presence of macropores, $>$50 nm. The average pore diameter and cumulative pore volume are assessed from the adsorption branch using the BJH (Figure 5 insets) or DFT (Supporting Information, Figure S1) models. The data in Table 1 demonstrate that the surface areas, average pore diameter, and cumulative pore volume of the aerogels are a direct function of the shape of the building block from which they were assembled. Impressively, the BET surface areas of rod or branched aerogels are twice as high as that of dot aerogels, which strongly indicates that these two distinctive morphologies (polymeric and colloidal) in metal chalcogenide aerogels have a significant impact on the surface area of resultant aerogels. This remarkable difference in surface areas is reflective of the different connectivity among the different-shaped building blocks, with the more interpenetrating structures obtained from rod and branched particles yielding higher surface areas.

Thus, the CdSe aerogels obtained from rods and branched particles have surface areas equivalent to that of an average silica aerogel (600 m^2/g)[10] when normalized for density differences (Table 1). The much lower surface area value of hyperbranched CdSe aerogels may be attributed to the larger size of the colloidal building block (Figure 1) and a decreased amount of thiolate ligands per nanoparticle resulting in fewer connection points and therefore a weaker network. TEM-EDS measurements of thiolate-capped hyperbranched nanoparticles indicate 6.6 atomic % S (attributed to thiolate) and 2.1 atomic % P (attributed to TOP/TOPO), whereas the other particle shapes have no detectable phosphorus and sulfur contents are on the order of 10−14 atomic %.[16] These data suggest that thiolate ligand exchange for TOP/TOPO functionalities, a key step in gel formation, is less facile for the hyperbranched particles.

The BJH modeled pore size distribution analyses (Figure 5, inset) from four kinds of CdSe aerogels all show a broad range of pores, from the mesopore to the macropore, and yield average values in the 13−35 nm range (Table 1). The main difference in the distribution curves is that, in the relatively large pore region, CdSe rod or branched aerogels show a similar upturn, while dot aerogels are relatively flat and hyperbranched aerogels exhibit a downturn. Similar profiles are obtained from the density functional theory model (assuming slit-shaped pore, Figure S1). Thus, the surface area differences noted for the different morphologies are reflective of the distribution of porosity within the aerogel and thus essentially mirror the cumulative pore volumes.

The band gap values of CdSe aerogels obtained from differently shaped building blocks were determined from diffuse reflectance UV/visible/NIR spectroscopy. All the spectra show sharp optical absorption onsets, and the band gap values were estimated from these onsets (Supporting Information, Figure S2). Compared with the band gap values of the respective building blocks from UV/visible transmission measurements, the nearly identical band gap of the CdSe aerogels indicates that the quantum confinement effects of the respective nanometer scale building blocks are almost fully maintained in the 3-D connected network (Table 1). This can be attributed to the low dimensional nature of the aerogel network.[34] A gradual decrease of the band gap values from the CdSe dot aerogel to the rod, branched, and hyperbranched aerogel is associated with the size increase of the building blocks and mirrors the data obtained on the original particles.

Emission properties of the differently shaped nanoparticle precursors (thiolate capped nanoparticles) and resultant aerogels were investigated using photoluminescence spectroscopy (Figure 6). Sharp band edge emission is apparent in the photoluminescence spectra of the MUA-capped dot, rod, and branched nanoparticle precursors, along with a broad peak to the red (1.6−1.9 eV) consistent with trap (mid-gap) states. Low-energy emission from mid-gap states is typical for thiolate-capped CdSe since thiolate ligands are effective hole traps.[35] The emission energy for the band edge PL of the resultant aerogels is nearly identical to the precursor nanoparticles, as is the general shape of the trap-state envelope, suggesting that the process of gelation and supercritical drying has not significantly altered the band gap (inferred from optical absorbance data) or the nature of the trap states (which presumably arise from residual thiolates). Importantly, the process does not appear to result in augmented surface defects that would quench the band edge emission entirely. The luminosity of the monoliths is thus apparent to the naked eye when viewed under UV excitation (Figure 2). The different emission colors are reflective of the energy of the band edge transition (Figure 6), with dots appearing green, rods yellow, and branched nanoparticles orange. Unique from the other shapes of building blocks investigated here, the emission of hyperbranched CdSe nanoparticles and their resultant aerogels is not detectable (Figures 2 and 6). This can be attributed to the large size of the CdSe hyperbranched nanoparticles and corresponding low degree of quantum confinement. To our knowledge, there are no reports of hyperbranched CdSe nanoparticles exhibiting photoluminescence properties.[28,36]

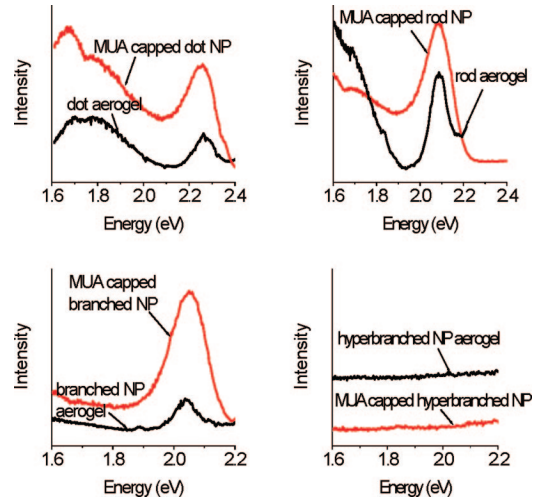

Figure 6. Photoluminescence measurements of the differently shaped CdSe nanoparticle building blocks (red) and the resultant aerogels (black).

CONCLUSIONS

Application of a general sol−gel methodology for the assembly of metal chalcogenide nanoparticles into aerogel frameworks has been demonstrated for differently shaped building blocks (dot, rod, branched, and hyperbranched). This has enabled the morphology of the aerogel to be sensitively adjusted between colloidal (dot aerogels) and polymeric (rod, branched aerogels) as well as dialing in intermediate morphologies

(hyperbranched aerogels). While the method itself "locks in" the inherent properties of the building block, so that the optical absorbance and PL signatures of the confined particles are retained in the monolithic assemblage, the surface area, porosity, and gel strength can be effectively tuned. Notably, polymeric CdSe aerogels based on rod or branched particles have superior porosity and gel strength, suggesting they may represent the most advantageous scaffolds for applications involving molecular transport (*e.g.*, sensing, photocatalysis).

METHODS

Synthesis. ***Materials.*** Trioctylphosphine oxide (TOPO, 90%), cadmium oxide (99.99%), selenium powder (99.5%), 11-mercaptoundecanoic acid (MUA, 95%), tetramethylammonium hydroxide pentahydrate (TMAH, 97%), tetranitromethane, and 2-carboxyethylphosphonic acid (CEPA 94%) were purchased from Aldrich. Trioctylphosphine (TOP, 97%) was purchased from Strem. *N*-Tetradecylphosphonic acid (98%) was purchased from Alfa-Aesar. Toluene, methanol, ethyl acetate, and ethyl alcohol were purchased from Fisher. Liquid CO_2 was supplied by Praxair. TOPO was distilled before using; other chemicals were used as received.

Synthesis of Dot-Shaped CdSe Nanoparticles. CdO powder (0.050 g, 0.37 mmol) was added to a mixture of TDPA (0.20 g, 0.72 mmol) and distilled TOPO (4.0 g, 10.3 mmol), heated at 150 °C, and kept under Ar flow for 30 min to remove residual water. Then the temperature was set to 320 °C, and the brownish mixture was left under Ar flow for 6−7 h, resulting in a colorless solution. The temperature was reduced to 150 °C, and a solution containing 0.032 g of selenium (0.30 mmol) in 2.5 mL of TOP was rapidly injected. The temperature was then raised at a rate of 10 °C per 10 min up to 230 °C, and the solution was kept at this temperature for 4 h before cooling down to 80 °C. Four milliliters of toluene was injected, and the particles precipitated with an excess of ethyl alcohol. To purify the particles, the solution was centrifuged and the sediment was redispersed in toluene. After a second precipitation with ethyl alcohol, the sediment was kept for further analysis.

Synthesis of Rod-Shaped CdSe Nanoparticles. CdO powder (0.15 g, 1.1 mmol) was added to a mixture of TDPA (0.70 g, 2.5 mmol) and distilled TOPO (4.0 g, 10.3 mmol) and heated at 150 °C under Ar flow for 30 min to remove residual water. Then the temperature was set to 320 °C and the solution left under Ar flow for 4 h to produce a colorless solution. The temperature was then reduced to 270 °C, and a solution of 0.095 g of selenium (1.1 mmol) in 1.5 mL of TOP was rapidly injected. The temperature was decreased to 230 °C, kept for 2 h, and then cooled to 80 °C. Isolation and purification were conducted as described for dot-shaped CdSe nanoparticles.

Synthesis of Branched CdSe Nanoparticles. CdO powder (0.15 g, 1.1 mmol), TDPA (1.0 g, 3.6 mmol), and distilled TOPO (3.0 g, 7.7 mmol) were heated at 150 °C under Ar flow for 30 min to remove residual water, then the temperature was increased to 320 °C for 1.5 h to yield a colorless solution. The temperature was reduced to 150 °C, and a solution of 0.095 g of selenium (1.1 mmol) in 1.5 mL of TOP was injected. The temperature was raised at a rate of 10 °C per 10 min up to 220 °C and maintained at this temperature for 2 h before cooling down to 80 °C. Isolation and purification were conducted as described for dot-shaped CdSe nanoparticles.

Synthesis of Hyperbranched CdSe Nanoparticles. CdO powder (0.15 g, 1.1 mmol), TDPA (1.0 g, 3.6 mmol), CEPA (0.05 g, 0.32 mmol), and distilled TOPO (3.0 g, 7.7 mmol) were heated together at 150 °C under Ar flow for 30 min to remove residual water. Then the temperature was set to 330 °C, and the brownish mixture was left under Ar flow for 1.5 h. This step resulted in a colorless solution. Next, 1.5 mL of neat TOP was injected into the system at 330 °C, followed by injection of a solution containing 0.064 g of selenium (0.60 mmol) in 3 mL of TOP. The reaction was maintained at 330 °C for 30 min before cooling down to 80 °C. Isolation and purification were conducted as described for dot-shaped CdSe nanoparticles.

MUA Capping of CdSe Nanoparticles, Gelation, and Aerogel Formation. To modify the CdSe nanoparticle surface, an MUA solution was prepared by dissolving 0.8 g if MUA (3.3 mmol) in 10 mL of methanol, with tetramethylammonium hydroxide pentahydrate (TMAH) added to achieve a system pH of 10.5−11. The solid precipitate of CdSe nanoparticles was then dispersed in the MUA solution and left stirring in a static Ar environment at 30 °C overnight. At room temperature, an excess amount of ethyl acetate was added to precipitate MUA-capped nanoparticles. The solution was centrifuged, and the sediment was redispersed in methanol. After a second precipitation with ethyl acetate, the sediment was dispersed in 10 mL of methanol for gelation.

Gelation was achieved by adding 20 μL of 3% tetranitromethane (TNM) in acetone solution to 2 mL aliquots of CdSe sols. The mixtures were shaken vigorously and subsequently allowed to sit undisturbed for gelation. The resulting wet gels were aged for 7 days under ambient conditions. Aged gels were exchanged with acetone 6−7 times over 3 days and then transferred to a SPI-DRY model critical point dryer where they were subsequently washed and immersed in liquid CO_2 over 6 h. The CO_2-exchanged gels were dried under supercritical conditions by raising the drier temperature to 39 °C, maintaining that temperature for 30 min, followed by venting of CO_2 gas to yield CdSe aerogels.

Characterization. ***Powder X-ray Diffraction.*** Powder X-ray diffraction (PXRD) analysis was employed to study the phase and crystallinity of the CdSe nanoparticles and resultant aerogels. A Rigaku RU 200B X-ray diffractometer (40 kV, 150 mW, Cu Kα radiation) with rotating anode was used for X-ray diffraction measurements. Powdered samples were deposited on a low background quartz (0001) holder coated with a thin layer of grease. X-ray diffraction patterns were identified by comparison to phases in the International Centre for Diffraction Data (ICDD) powder diffraction file (PDF) database (release 2000).

Transmission Electron Microscopy. Transmission electron microcopy (TEM) was employed to study the four different CdSe building blocks and the morphology of the resultant aerogels. The TEM analyses were conducted in the bright field mode using a JEOL FasTEM 2010 HR TEM analytical electron microscope operating at an accelerating voltage of 200 kV. Particle samples were prepared by depositing a drop of a dilute toluene dispersion of CdSe nanocrystals on carbon-coated copper grids and subsequently evaporating the solvent. Aerogel samples were prepared on carbon-coated copper grids by first grinding the aerogel to fine powders and then pressing the TEM grid onto the dried powder. Semiqualitative elemental compositions of differently shaped CdSe nanoparticles along with the resultant aerogels were obtained using an *in situ* energy dispersive spectroscopy (EDS) unit (EDAX, Inc.) attached to the transmission electron microscope. K shell electron emissions were analyzed for Cd, Se, S, and P.

Surface Area Analysis and Porosimetry. The surface areas of CdSe aerogels were obtained by applying the BET model to nitrogen adsorption/desorption isotherms acquired at 77 K on a Micromeritics ASAP 2010 surface area analyzer. Powdered CdSe aerogel samples were degassed at 100 °C for 48 h prior to the analysis, employing a 30 s equilibrium interval and a 5 cc dose for a total running time of about 13 h. The data were fit by using the Brunauer−Emmett−Teller (BET) model to determine the surface areas of the aerogels. The average pore diameter and cumulative pore volume were calculated by using the Barrett−Joyner−Halenda (BJH) model based on cylinder pore geometry. The density function theory model, based on slit pore geometry, was also employed to analyze the pore distribution. Three independently prepared samples from each kind of CdSe aerogel were analyzed to obtain average surface area and porosity values.

Silica Equivalent Surface Area Calculation. The calculation is based on a relative density method. The average silica density is the aver-

age density of quartz (2.65 mg/cc), tridymite (2.31 mg/cc), and cristobalite (2.33 mg/cc), 2.43 mg/cc. The CdSe wurzite density is 5.81 mg/cc. The actual surface area value of a typical CdSe dot aerogel is 118 m^2/g. The silica equivalence of a dot aerogel is therefore 118 (m^2/g)* 5.81/2.43 = 282 m^2/g. A similar approach was used to compute silica equivalence values for rod, branched, and hyperbranched aerogels.

Optical Absorption Measurements. Optical absorption measurements of MUA-capped CdSe nanoparticles in methanol were conducted on a Hewlett-Packard (HP) 8453 spectrophotometer. A dilute CdSe nanoparticle suspension was analyzed against a methanol blank in the region from 400 to 700 nm. A Jasco V-570 UV/vis/NIR spectrophotometer equipped with an integrating sphere was used to measure the optical diffuse reflectance of the resultant CdSe aerogels. Powdered aerogel samples were evenly spread on a sample holder preloaded with a reflectance standard and measured from 200 to 1500 nm. The band gaps of the samples were estimated from the onset of absorption in data converted from reflectance.[37,38]

Photoluminescence Measurements. Emission properties of the CdSe nanoparticle precursors and corresponding aerogels were investigated using photoluminescence spectroscopy. A Cary Eclipse (Varian, Inc.) fluorescence spectrometer with 5 nm excitation and emission slits was used for photoluminescence studies. A dilute MUA-capped CdSe nanoparticle suspension in methanol was placed in a 10 mm quartz optical cell, and analyses were done under ambient conditions. Powdered aerogel samples were sealed in evacuated quartz tubes, and analyses were conducted at liquid nitrogen temperature.

Acknowledgment. We thank Yi Liu for the assistance with TEM measurements. This work was supported by the National Science Foundation (DMR-0701161) and the donors of the Petroleum Research Fund, administered by the American Chemical Society (AC-43550). Electron microscopy was acquired in the WSU Central Instrumentation Facility on a JEOL 2010F purchased under NSF Grant DMR-0216084.

Supporting Information Available: Pore size distributions of CdSe aerogels from the density functional theory model and band gap measurements of the differently shaped CdSe building blocks and the resultant aerogels. This material is available free of charge *via* the Internet at http://pubs.acs.org.

REFERENCES AND NOTES

1. Murray, C. B.; Norris, D. J.; Bawendi, M. G. Synthesis and Characterization of Nearly Monodisperse CdE (E = S, Se, Te) Semiconductor Nanocrystallites. *J. Am. Chem. Soc.* **1993**, *115*, 8706–8715.
2. Manna, L.; Scher, E. C.; Alivisatos, P. A. Synthesis of Soluble and Processable Rod-, Arrow-, Teardrop-, and Tetrapod-Shaped CdSe Nanocrystals. *J. Am. Chem. Soc.* **2000**, *122*, 12700–12706.
3. Mikulec, F. V.; Kuno, M.; Bennati, M.; Hall, D. A.; Griffin, R. G.; Bawendi, M. G. Organometallic Synthesis and Spectroscopic Characterization of Manganese-Doped CdSe Nanocrystals. *J. Am. Chem. Soc.* **2000**, *122*, 2532–2540.
4. Aldana, J.; Wang, Y. A.; Peng, X. Photochemical Instability of CdSe Nanocrystals Coated by Hydrophilic Thiols. *J. Am. Chem. Soc.* **2001**, *123*, 8844–8850.
5. Urban, J. J.; Talapin, D. V.; Shevchenko, E. V.; Murray, C. B. Self-Assembly of PbTe Quantum Dots into Nanocrystal Superlattices and Glassy Films. *J. Am. Chem. Soc.* **2005**, *128*, 3248–3255.
6. Collier, C. P.; Vossmeyer, T.; Heath, J. R. Nanocrystal Superlattices. *Annu. Rev. Phys. Chem.* **1998**, *49*, 371–404.
7. Redl, F. X.; Cho, K.-S.; Murray, C. B.; O'Brien, S. Three-Dimensional Binary Superlattices of Magnetic Nanocrystals and Semiconductor Quantum Dots. *Nature* **2003**, *423*, 968–971.
8. Shevchenko, E. V.; Talapin, D. V.; Kotov, N. A.; O'Brien, S.; Murray, C. B. Structural Diversity in Binary Nanoparticle Superlattices. *Nature* **2006**, *439*, 55–59.
9. Shevchenko, E. V.; Talapin, D. V.; Murray, C. B.; O'Brien, S. Structural Characterization of Self-Assembled Multifunctional Binary Nanoparticle Superlattices. *J. Am. Chem. Soc.* **2006**, *128*, 3620–3637.
10. Hüsing, N.; Schubert, U. Aerogel-Airy Materials: Chemistry, Structure, and Properties. *Angew. Chem., Int. Ed.* **1998**, *37*, 22–45.
11. Baumann, T. F.; Kucheyev, S. O.; Gash, A. E.; Satcher, J. H. J. Facile Synthesis of a Crystalline, High-Surface-Area SnO_2 Aerogel. *Adv. Mater.* **2005**, *17*, 1546–1548.
12. Gash, A. E.; Satcher, J. H. J.; Simpson, R. L. Strong Akaganeite Aerogel Monoliths Using Epoxides: Synthesis and Characterization. *Chem. Mater.* **2003**, *15*, 3268–3275.
13. Long, J. W.; Rhodes, C. P.; Young, A. L.; Rolison, D. R. Ultrathin, Protective Coatings of Poly(*o*-pheylenediamine) as Electrochemical Proton Gates: Making Mesoporous MnO_2 Nanoarchitectures Stable in Acid Electrolytes. *Nano Lett.* **2003**, *3*, 1155–1161.
14. Rolison, D. R. Catalytic Nanoarchitectures—The Importance of Nothing and the Unimportance of Periodicity. *Science* **2003**, *299*, 1698–1701.
15. Rolison, D. R.; Dunn, B. Electrically Conductive Oxide Aerogels: New Materials in Electrochemistry. *J. Mater. Chem.* **2001**, *11*, 963–980.
16. Arachchige, I. U.; Brock, S. L. Sol−Gel Assembly of CdSe Nanoparticles to Form Porous Aerogel Networks. *J. Am. Chem. Soc.* **2006**, *128*, 7964–7971.
17. Arachchige, I. U.; Brock, S. L. Highly Luminescent Quantum-Dot Monoliths. *J. Am. Chem. Soc.* **2007**, *129*, 1840–1841.
18. Kalebaila, K. K.; Georgiev, D. G.; Brock, S. L. Synthesis and Characterization of Germanium Sulfide Aerogels. *J. Non-Cryst. Solids* **2006**, *352*, 232–240.
19. Mohanan, J. L.; Brock, S. L. A New Addition to the Aerogel Community: Unsupported CdS Aerogels with Tunable Optical Properties. *J. Non-Cryst. Solids* **2004**, *350*, 1–8.
20. Mohanan, J. L.; Brock, S. L. CdS Aerogels: Effect of Concentration and Primary Particle Size on Surface Area and Opto-electronic Properties. *J. Sol−Gel Sci. Technol.* **2006**, *40*, 341–350.
21. Arachchige, I. U.; Brock, S. L. Sol−Gel Methods for the Assembly of Metal Chalcogenide Quantum Dots. *Acc. Chem. Res.* **2007**, *40*, 801–809.
22. Brock, S. L.; Arachchige, I. U.; Kalebaila, K. K. Metal Chalcogenide Gels, Xerogels and Aerogels. *Comm. Inorg. Chem.* **2006**, *27*, 103–106.
23. Mohanan, J. L.; Arachchige, I. U.; Brock, S. L. Porous Semiconductor Chalcogenide Aerogels. *Science* **2005**, *307*, 397–400.
24. Bag, S.; Trikalitis, P. N.; Chupas, P. J.; Armatas, G. S.; Kanatzidis, M. G. Porous Semiconducting Gels and Aerogels from Chalcogenide Clusters. *Science* **2007**, *317*, 490–493.
25. Arachchige, I. U.; Mohannan, J. L.; Brock, S. L. Sol-Gel Processing of Semiconducting Metal Chalcogenide Xerogels: Influence of Dimensionality on Quantum Confinement Effects in a Nanoparticle Network. *Chem. Mater.* **2005**, *17*, 6644–6650.
26. Yu, H.; Bellair, R.; Kannan, R. M.; Brock, S. L. Engineering Strength, Porosity, and Emission Intensity of Nanostructured CdSe Networks by Altering the Building Block Shape. *J. Am. Chem. Soc.* **2008**, *130*, 5054–5055.
27. Peng, Z. A. P.; Peng, X. Mechanisms of the Shape Evolution of CdSe Nanocrystals. *J. Am. Chem. Soc.* **2001**, *123*, 1389–1395.
28. Kanaras, A. G.; Soennichsen, C.; Liu, H.; Alivisatos, A. P. Controlled Synthesis of Hyperbranched Inorganic Nanocrystals with Rich Three-Dimensional Structures. *Nano Lett.* **2005**, *5*, 2164–2167.
29. Brinker, C. J.; Scherer, G. W. *Sol−Gel Science*; Academic Press: San Diego, CA, 1990.
30. Mokari, T.; Rothenberg, E.; Popov, I.; Costi, R.; Banin, U. Selective Growth of Metal Tips onto Semiconductor Quantum Rods and Tetrapods. *Science* **2004**, *304*, 1787–1790.

31. Halpert, J. E.; Porter, V. J.; Zimmer, J. P.; Bawendi, M. G. Synthesis of CdSe/CdTe Nanobarbells. *J. Am. Chem. Soc.* **2006**, *128*, 12590–12591.
32. Gregg, S. J.; Sing, K. S. W. *Adsorption, Surface Area and Porosity*, 2nd ed.; Academic: New York, 1982.
33. Webb, P. A.; Orr, C. *Analytical Methods in Fine Particle Technology*; Micromeritics Instrument Corp.: Norcross, GA, 1997.
34. Emmerling, A.; Fricke, J. Small Angle Scattering and the Structure of Aerogels. *J. Non-Cryst. Solids* **1992**, *145*, 113–120.
35. Alivisatos, A. P. Semiconductor Clusters, Nanocrystals, and Quantum Dots. *Science* **1996**, *271*, 933–937.
36. Zhong, H.; Zhou, Y.; Yang, Y.; Yang, C.; Li, Y. Synthesis of Type II CdTe−CdSe Nanocrystal Heterostructured Multiple-Branched Rods and Their Photovoltaic Applications. *J. Phys. Chem. C* **2007**, *111*, 6538–6543.
37. Wendlandt, W. W.; Helcht, H. G. *Chemical Analysis: Reflectance Spectroscopy*; Wiley-Interscience: New York, 1966; Vol. 21.
38. Tandon, S. P.; Gupta, J. P. Measurement of Forbidden Energy Gap of Semiconductors by Diffuse Reflectance Technique. *Phys. Status Solidi* **1970**, *38*, 363–367.